RSC Advances

PAPER

View Article Online
View Journal | View Issue

Cite this: *RSC Adv.*, 2022, **12**, 23416

Fischer–Helferich glycosidation mechanism of glucose to methyl glycosides over Al-based catalysts in alcoholic media†

Mengting Yu,[a] Yao Li,[b] Cheng Zhang,[c] Huaying Luo,[c] Chengsheng Ge,[a] Xiaobin Chen,[a] Lanlan Fu,[a] Zhaoyang Ju *[ac] and Xiaoqian Yao*[b]

The Fischer–Helferich glycosidation reaction is generally the initial step in the conversion of glucose to levulinate in alcohol media. However, the relevant molecular mechanism catalyzed by Al-based catalysts is still not well understood. In this work, the reaction mechanism of the glycosidation from glucose to methyl glycosides catalyzed by Al^{3+} coordinated with methanol/methoxyl was investigated through density functional theory (DFT) calculations. The whole reaction process includes ring-opening, addition, and ring-closure events. The addition of methanol to the ring-opening structure of glucose makes the electronegativity of C1 site stronger to proceed with the following ring-closure reaction. Among the 28 kinds of ways of ring-closure reaction, the most preferred way is to close the loop through the six-membered ring (O5–C1) to generate methyl glucoside (MDGP). The rate-determining step is the ring-closure and the Al^{3+} shows a great catalytic effect which is mainly reflected in coordinating with the solvents to transfer protons. The results would be helpful to understanding the Fischer–Helferich glycosidation mechanism catalyzed by Al-based catalysts and comprehend the conversion of glucose to high value-added chemicals.

Received 27th June 2022
Accepted 10th August 2022

DOI: 10.1039/d2ra03945a

rsc.li/rsc-advances

1. Introduction

The conversion of biomass resources to valuable platform chemicals is of critical importance according to the diminishing fossil fuels and global warming effects.[1,2] Among the various biomass-derived products, glucose is the monomer unit of cellulose which could produce a variety of valuable chemicals, such as 5-hydroxymethyl-furfural and levulinates.[3–5] The Fischer–Helferich glycosidation is a simple and cheap method to render alkyl and aryl glycoside from sugars which is also prevalent in the conversion of glucose to levulinate.[6] Besides, the carbohydrate derivatives have been widely used in food emulsifiers, cosmetic surfactants, and solvents for membranes.[7]

As a promising approach, alcoholysis technology has been maturely applied for the conversion of lignocellulose to platform chemicals due to its various advantages. Compared with the conversion of glucose to biofuels in the water medium, alcoholysis could avoid wasting water and decrease humins or chars.[8,9] Moreover, the alkyl levulinate generated in alcohol gives a higher yield than levulinic acid obtained in water.[10,11] In the previous work, Deng *et al.* reported that abundant products such as glucose, fructose, and methyl glucoside (MDGP), were detected in methanol, and the yield of MDGP was relatively high because glucose tends to undergo Fischer–Helferich glycosidation to generate MDGP.[12] In 2019, Chung *et al.* described that decyl glucoside was synthesized by direct glucosidation from glucose in 1-decanol using zeolite catalysts.[13] The glucose could form alkyl glucoside in the alcohol system through Fischer–Helferich glycosidation which is described in Scheme 1.[14,15] Fischer–Helferich glycosidation is one of the most promising choices to prepare alkyl or aryl glycosides from sugars. Most studies have concentrated on the conversion experiments and development of high-efficiency catalysts due to the wide application of high value-added alkyl glucosides. However, the detailed reaction mechanism of Fischer–Helferich glycosidation remains ambiguous.

[a]*College of Chemical & Material Engineering, Quzhou University, Quzhou 324000, P. R. China. E-mail: jzy@qzc.edu.cn*

[b]*CAS Key Laboratory of Green Process and Engineering, Beijing Key Laboratory of Ionic Liquids Clean Process, State Key Laboratory of Multiphase Complex Systems, Institute of Process Engineering, Chinese Academy of Sciences, Beijing 100190, P. R. China. E-mail: xqyao@ipe.ac.cn*

[c]*Xianhe Co., Ltd, Quzhou 324000, P. R. China*

† Electronic supplementary information (ESI) available. See https://doi.org/10.1039/d2ra03945a

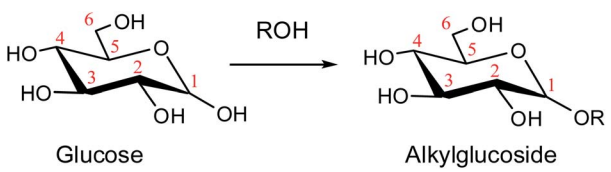

Scheme 1 The glycosidation of glucose to alkyl glucoside.

In the past decades, numerous kinds of catalysts were used for the conversion of glucose in the alcohol media, and the corresponding glycosidation reaction was indicated based on the intermediate alkyl glucosides.[11,16] As one kind of sustainable clean catalysts, Al-based catalysts, such as $Al_2(SO_4)_3$, $AlCl_3$, and $AlPW_{12}O_{40}$ are efficient for the conversion of biomass carbohydrates in the alcoholic solvents.[17,18] Various coordination structures could be formed with the solvents to catalyze many reactions, such as the sugar isomerization, Fischer–Helferich glycosidation, and the dehydration of fructose.[19] He *et al.* investigated the predominant coordination of cyclic β-D-glucose to $[Al(OH)(aq)]^{2+}$ and $[Al(OH)_2(aq)]^{+}$ ions and gained many stable coordination species, which may aid in understanding the glucose isomerization.[20] Norton *et al.* reported that the hydrolyzed Al^{3+} complex $[Al(H_2O)(OH)_2]^{1+}$ was the active species in the glucose isomerization.[21] Furthermore, Saravanamurugan *et al.* proposed that bifunctional Lewis and Brønsted acid sites in the Al-based catalyst structures were one of the most important reasons to catalyze the glycosidation.[22] Recently, as a promising bifunctional catalyst for biomass carbohydrate transformation to methyl levulinate, $AlPW_{12}O_{40}$ has shown superior activity and the bifunctional Lewis and Brønsted acid site structure $[Al(CH_3O)_2(CH_3OH)_2]^{+}$ can be detected by GC-MS experiments.[23] However, the detailed glycosidation mechanism of glucose to methyl glycosides catalyzed by Al-based catalyst is still not clear.

To understand the fundamental reaction mechanism of Fischer–Helferich glycosidation of glucose to methyl glycosides catalyzed by Al-based catalysts in methanol solvent, we investigated in detail the reaction pathways of glucose to methyl glycosides over $[Al(CH_3O)_2(CH_3OH)_2]^{+}$ catalyst by DFT calculations in this work. In the Fischer–Helferich glycosidation process, there are mainly three steps including the ring-opening of glucose, addition, and ring closure reaction. The reaction pathways were explored in detail and activation barriers of each step were compared. The reaction pathways without catalyst and catalyzed by Al-based catalysts in methanol solvent had been also probed. Finally, the Fischer–Helferich glycosidation mechanism of glucose catalyzed by Al-based catalysts had been proposed. The calculated results would provide comprehensive information to understand the glycosidation of glucose to alkyl glycosides in alcoholic solution.

2. Computational method

All the calculations were carried out by using the M06-2X functional,[24] which is proposed to be one of the best functionals to accurately calculate energy barrier, with the standard 6-311+G** basis set and Grimme's D3 dispersion corrections,[25] as implemented in Gaussian 09 software package.[26] The geometries for the reactants, transition states, and products were fully optimized without any constraints in the gas phase and generated by CYL view.[27] To account for the solvent effects, single-point calculations were performed in a methanol dielectric by using the SMD solvation model.[28] Vibrational frequency calculations were also carried out to verify the optimized structures as minima (zero imaginary frequency) or first-order saddle points (one imaginary frequency) and to provide free energies at 298.15 K, 1 atm. Gibbs free energies were calculated by the sum of energies in the SMD solvent and thermal correction to Gibbs free energies at M06-2X-D3/6-311+G** level. The intrinsic reaction coordinate (IRC) pathways[29] of transition states have been traced to confirm that each of them connects the desired reactant and product. Furthermore, the potential energy surface (PES) scans[30] were performed to search for the TS structures. The activation energy (G_a) which is the energy barrier and reaction energy (G_r) of the systems are defined as follows:

$$G_a = G_{TS} - G_R,\ G_r = G_P - G_R \quad (1)$$

where G_{TS}, G_R, G_P represent the Gibbs free energies of transition state, reactant, and product. Noncovalent interactions (NCIs) were characterized by using Reduced Density Gradients (RDGs) approach[31] which can be defined as the following:

$$s = \frac{1}{2(3\pi^2)^{1/3}} \frac{|\nabla\rho|}{\rho^{4/3}} \quad (2)$$

where ρ stands for the electron density and $|\nabla\rho|$ represents the norm of electron density gradient vector. The RDG is typically plotted against $\mathrm{sign}(\lambda_2)\rho$ in a scattering diagram where the $\mathrm{sign}(\lambda_2)$ is the sign of the second curvature of the electron density. The topological properties were generated by Multiwfn program[32] with the wave functions in M06-2X-D3/6-311+G** level.

3. Results and discussion

For the Fischer–Helferich glycosidation reaction, it is prevalent in the conversion experiments of glucose under alcohol solvent.[33] The detailed reaction pathways were not expounded in most of the studies. The Mayer bond order is a natural extension of the Wiberg bond order, which has proved extremely useful in bonding analysis.[34] The Mayer bond order analysis has been made for the C–O of glucose which was shown in Fig. S1.† The Mayer bond order of C1–O5 (the C–O in the ring) and C1–O1 (the C–O in hydroxyl) are 0.86, and 1.36, respectively. It means the C1–O5 bond is easier cleavage than C1–O1. For the direct etherification reaction of methanol (the oxygen of CH_3OH attacks C1 of glucose), the potential energy 3D surface scan was made in Fig. S2.† When the methanol attacks the C1 site of glucose, the C1–O1H1 bond length would increase and attract the proton of methanol for dehydration. It can be found that the relative energy will increase for direct etherification and there are also no saddle points in the 3D surface scan. In addition, the ring-opening of glucose with a linear hemiacetal structure (IM1) can be detected in the initial reaction stage by using radioactive sugars.[35,36] Based on previous research on the glycosidation of glucose to MDGP,[37,38] it is generally recognized that the conversion occurs through the methanol addition to the ring-opening structure of glucose which is shown in Scheme 2. Therefore, the whole glycosidation mechanism generally includes ring-opening, addition, and ring closure events. In the

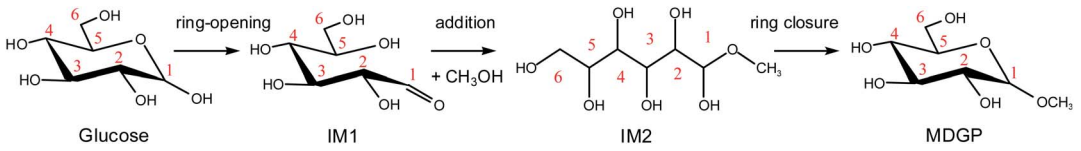

Scheme 2 The general mechanism for the glycosidation of glucose to methyl glycoside.

following sections, we will discuss the mechanism of glucose to MDGP without and with $[Al(CH_3O)_2(CH_3OH)_2]^+$ catalyst.

3.1 The ring-opening reaction of glucose

The ring-opening reaction step where the proton from the hydroxyl group at C1 transfers to O6 atom has been reported by some theoretical studies like the isomerization of sugars.[39,40] Firstly, the ring-opening reaction of glucose without catalyst was calculated and shown in Fig. 1. The proton at O1 directly transfers to O5 and the length of C1–O5 bond gradually increases cleavage with the structure of TSa. The product (IM1) of the ring-opening reaction will be formed with a 47.1 kcal mol^{-1} energy barrier. This process is an endothermic reaction of 8.0 kcal mol^{-1}.

Saravanamurugan *et al.* reported that Al-based zeolites with combined Brønsted and Lewis acid sites could catalyze the glucose isomerization at relatively low temperatures.[22] In aqueous media, the distribution of hydrolyzed $AlCl_3$ species depends on many parameters, *e.g.*, the concentration of $AlCl_3$, pH value, temperature, and so on.[41] It is generally believed that Al^{3+} exists in the form of (1) hexa-coordinated $[Al(aq)]^{3+}$ in strong acid solution (pH < 3.0), (2) $[Al(OH)_2(H_2O)_{n-2}]^+$, and $[Al(OH)(H_2O)_{n-1}]^{2+}$ around a pH of 4.0 (where n is the coordination number), (3) $[Al(OH)(H_2O)_{n-1}]^{2+}$ as well as $[Al(OH)_4]^-$ at pH values of 5.2–6.7, (4) a tetrahedral $[Al(OH)_4]^-$ structure (pH > 7.0).[42,43] Theoretical and experimental research studies indicate that the four-coordination $[Al(OCH_3)_2(CH_3OH)_2]^+$ plays a crucial role in the conversion of sugars after the typical stable $[Al(CH_3O)_m(CH_3OH)_n]^{3-m}$ (m = 0–6, $m + n \leq 6$) species were

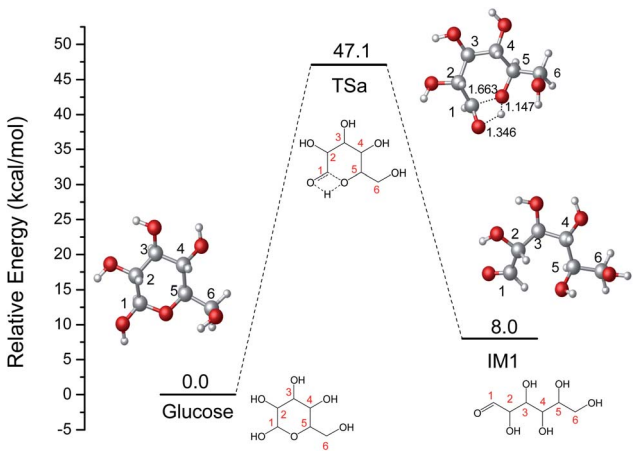

Fig. 1 The potential energy (kcal mol^{-1}) profile with the structures of reactant, transition state, and product for the ring-opening of glucose without catalyst (bond distances in Å).

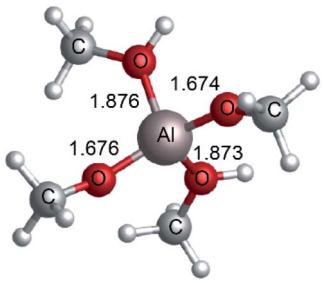

Fig. 2 The structure of $[Al(CH_3O)_2(CH_3OH)_2]^+$ optimized at M06-2X-D3/6-311+G** level (bond length in Å).

calculated.[19] To gain a further understanding of the Fischer–Helferich glycosidation mechanism, the $[Al(CH_3O)_2(CH_3OH)_2]^+$ structure (Fig. 2) containing both bifunctional Lewis and Brønsted acid sites was used and reported in our previous study.[19] To investigate the ring-opening reaction of glucose catalyzed by $[Al(CH_3O)_2(CH_3OH)_2]^+$, the energy profile and reactants, transition states, and products of this process were probed and presented in Fig. 3. For the ring-opening reaction, the O1H1 of glucose was activated by $[Al(CH_3O)_2(CH_3OH)_2]^+$. In R1 ($[(\eta^1{}_{O1}\text{-Glu})Al(CH_3O)_2(CH_3OH)_2]^+$), the Al^{3+} interacts with the hydroxyl group (O1) at a Al–O bond length of 2.031 Å, and the methanol coordinated with Al^{3+} forms H-bonds with O5 at a distance of 1.769 Å. The H1 transfers to the methoxy group coordinated with Al^{3+} *via* TS1 with a barrier of 4.5 kcal mol^{-1}, which means it is easy to undergo the first step, and it will form P1 (H1 of glucose transfers to OCH_3 of $[Al(CH_3O)_2(CH_3OH)_2]^+$). This step is exothermic by about 4.6 kcal mol^{-1}. The P1 and R2 are isomers in differently spatial position. Then, the hydrogen of methanol coordinated with Al^{3+} transfers to O5, and the length of C1–O5 bond gradually becomes longer (TS2). Finally, the ring-opening of the glucose (P2) was formed with the C1–O5 bond cleavage. The second step involves a free energy barrier of 10.1 kcal mol^{-1} which is 5.5 kcal mol^{-1} higher than the first step. The ring-opening catalyzed by $[Al(CH_3O)_2(CH_3OH)_2]^+$ shows that $[Al(CH_3O)_2(CH_3OH)_2]^+$ can significantly decrease the energy barrier through the hydrogen transfer of methanol coordinated with Al^{3+}.

3.2 Addition reaction

The ring-opening structures of glucose (IM1) and MDGP (IM2) are two important intermediates in the Fischer–Helferich glycosidation.[44,45] As a useful method to predict the reactive site of the molecular surface, quantitative molecular surface analysis of electronic potential (ESP) had been widely used in many DFT studies.[46,47] Based on the structure of reactants optimized at

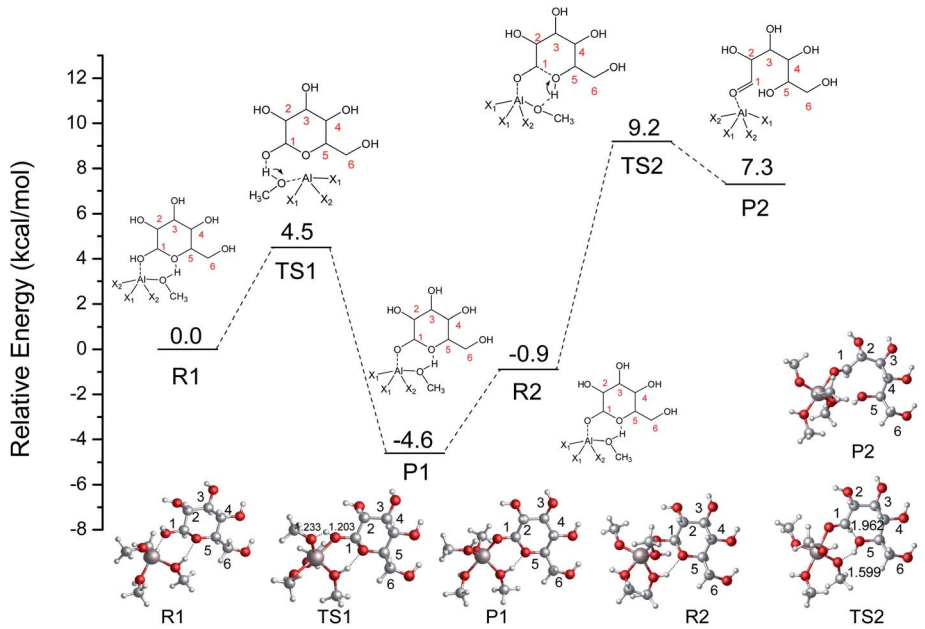

Fig. 3 The potential energy (kcal mol^{-1}) profile with the structures of reactants, transition states, and products for the ring-opening of glucose catalyzed by $[Al(CH_3O)_2(CH_3OH)_2]^+$ (X_1 = CH_3OH, X_2 = CH_3O, bond distances in Å).

M06-2X-D3/6-311+G** level, the ESP of IM1 and IM2 had been analyzed and listed in Fig. 4. The ESP surface minimum of IM1 and IM2 is located in the O1 area which is −0.046 and −0.070 a.u., respectively. In the IM2, the addition of methanol makes the ESP around the O1 area more negative to undergo the following ring-closure reaction. Besides, the electropositive region of IM1 and IM2 are located around the O6 site. However, the change (0.003 a.u.) is not obvious when the methanol was added to IM1. As one of the most widely used methods to accurately describe the charge distribution in the chemical system, the natural population analysis (NPA) charge was also calculated.[48] The NPA charge of IM1 and IM2 was calculated and summarized in Table S1.† In IM2, the NPA charge of C1–C6 are 0.430, 0.073, 0.078, 0.098, 0.074, and −0.054 a.u. The most positive and negative sites are located in C1 and C6, respectively. These changes in the chemical properties when the methanol was added in IM1 would be beneficial for the following ring-closure reaction. The subsequent step is the addition reaction where the ring-opening form glucose (IM1) is transformed into IM2 (Fig. 5). A transition state (TSb) is located to connect Rb (IM1) and Pb (IM2) with a reasonable activation barrier of 35.5 kcal mol^{-1}. In the geometry of TSb, the oxygen of methanol is found to be close to the C1 with a distance of 1.58 Å in the four-membered ring transition structure. In the addition reaction step, the H-transfer assisted by two MeOH molecules had been probed and combined in Fig. 5. A six-membered transition state can be formed with 19.8 kcal mol^{-1} energy barrier which is lower than that of Rb–Pb.

To explore the addition reaction catalyzed by $[Al(CH_3O)_2(CH_3OH)_2]^+$, the energy profile with the structures for two different pathways in the addition reaction is shown in Fig. 6. In the R3–P3 reaction pathway, the proton (hydroxyl) of CH_3OH coordinated with $[Al(CH_3O)_2(CH_3OH)_2]^+$ transfers to O1 of IM1, and the OCH_3 coordinated with Al^{3+} was added to C1 of IM1.

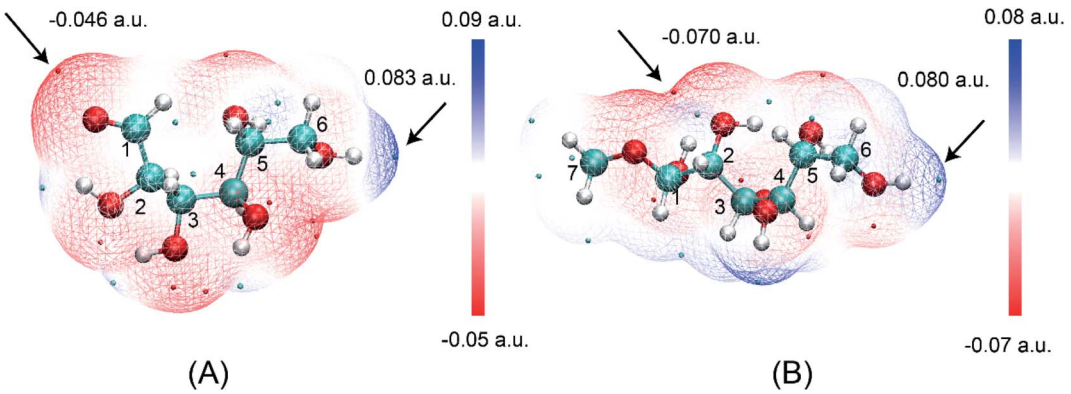

Fig. 4 The electrostatic potential on the van der Waals surfaces of (A) IM1 and (B) IM2.

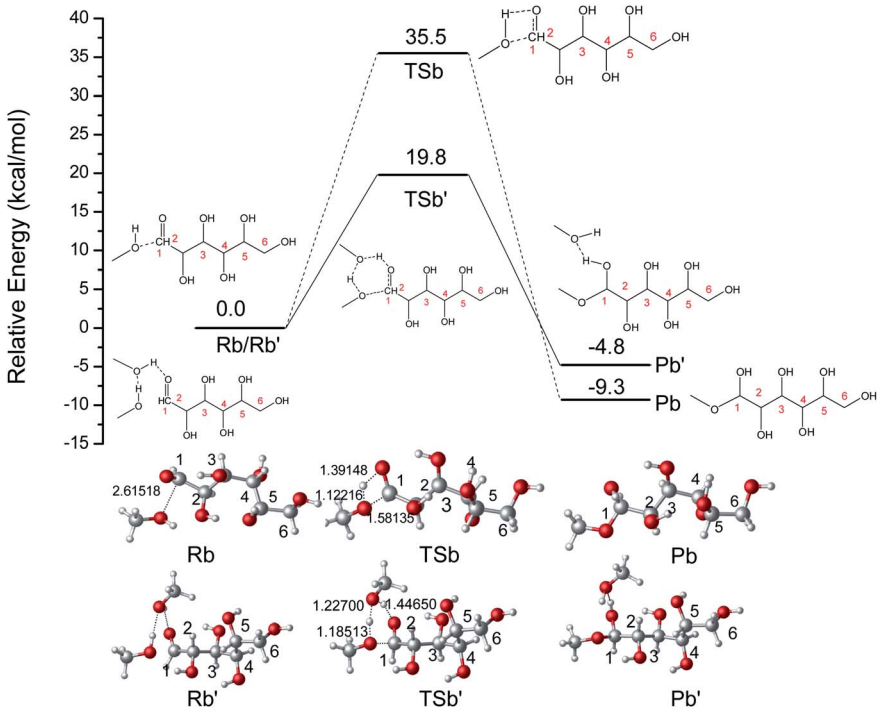

Fig. 5 The potential energy (kcal mol^{-1}) profile with the structures of reactant, transition state, and product for the addition reaction without catalyst. (bond distances in Å).

The IM1 was active by the coordination of $[Al(CH_3O)_2(CH_3OH)_2]^+$ (R3). In TS3, the hydrogen of methanol coordinated with Al^{3+} transfers to the O1, and the methoxy attacks C1 with only a 14.3 kcal mol^{-1} energy barrier. This process is exothermic by 2.8 kcal mol^{-1}. In another reaction pathway (R3′–P3′), H-bonds initially can be formed between Al^{3+} and O5, then H (hydroxyl)

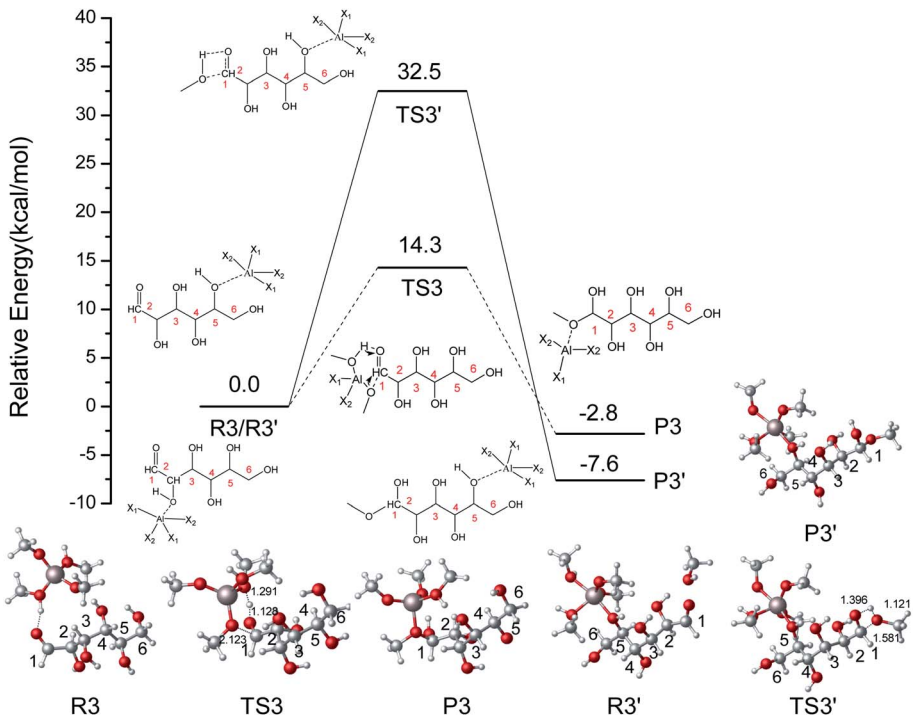

Fig. 6 The potential energy (kcal mol^{-1}) profile with the structures of reactants, transition states, and products for two different pathways in the addition reaction catalyzed by $[Al(CH_3O)_2(CH_3OH)_2]^+$. ($X_1 = CH_3OH$, $X_2 = CH_3O$, bond distances in Å).

of CH_3OH transfers to O1, and the methoxy was added to C1 of IM1. The energy barrier of R3′–P3′ is 32.5 kcal mol^{-1} and higher than that of R3–P3. Therefore, the role of Al^{3+} is mainly reflected through the hydrogen transfer of coordinated methanol. In the Fischer–Helferich glycosidation, the energy barrier of the addition reaction (R3–P3) is higher than that of the ring-opening step.

3.3 Ring-closure reaction

Cyclic anhydrosugars are important intermediates in synthetic carbohydrate chemistry.[49] Four different main rings, *i.e.*, three-, four-, five-, and six-membered ring, can be formed due to the six hydroxyls in IM2. For the three-membered rings, there are ten different kinds of ways which are the connection of O1–C2, O2–C3, O3–C4, O4–C5, O5–C6, O2–C1, O3–C2, O4–C3, O5–C4, and O6–C5, respectively. For the four-membered ring, there are eight different types of ways which are O1–C3, O2–C4, O3–C5, O4–C6, O6–C4, O5–C3, O4–C2, and O3–C1. In the five-membered ring reactions, important intermediates would be produced such as methyl fructoside which can provide a referable pathway in the alcohol system. There are six different kinds of ways which are O1–C4, O2–C5, O3–C6, O6–C3, O5–C2, and O4–C1. Also, for the six-membered ring to form meaningful products like MDGP, there are four different ways which are O1–C5, O2–C6, O6–C2, and O5–C1. As a result, there are 28 kinds of ways in the ring-closure reaction step. We had calculated all of the ring-closure reactions discussed above. The corresponding energies and the structures of products are summarized in Table 1. The H5 of O5 transfers to O1H1 and the O5–C1 bond will be formed to produce MDGP based on the pathway with the lowest energy barrier. The detailed discussions of the various ring-closure reactions were put in ESI.†

Based on the results mentioned above, the lowest energy barrier (52.8 kcal mol^{-1}) is for the O5–C1 six-membered ring closure reaction which can produce MDGP. After probing the reaction pathways of the ring-closure reaction without a catalyst, we choose the way of O5–C1 six-membered ring closure with lowest energy barrier and the reaction mechanism catalyzed by $[Al(CH_3O)_2(CH_3OH)_2]^+$ had been investigated based on the DFT calculations. The lowest energy barrier of IM2 through O5–C1 ring-closure reaction to MDGP is demonstrated in Fig. 7. Initially, H-bonds were formed between Al^{3+} and O1 with a 1.960

Table 1 The computed activation energy (G_a), reaction energy (G_r), and the structures of products in the three-(1–10) four-(11–18) five-(19–24) and six-(25–28) membered ring-closure reaction from IM2. (unit kcal mol^{-1})

Entry	Ring-closure	Ways	G_a	G_r	Structure of products
1	Three-	O1–C2	72.3	22.7	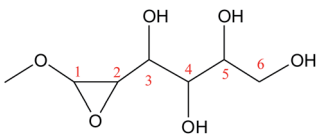
2		O2–C1	53.6	16.3	
3		O2–C3	64.8	15.4	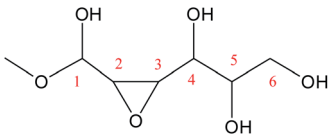
4		O3–C2	78.5	21.8	
5		O3–C4	80.3	17.0	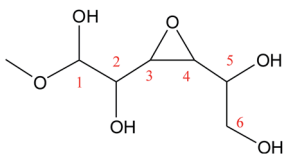
6		O4–C3	75.0	19.6	
7		O4–C5	73.7	18.3	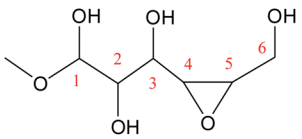
8		O5–C4	72.5	16.5	
9		O5–C6	74.9	16.2	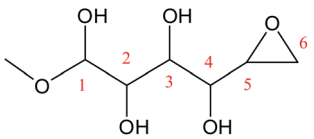
10		O6–C5	73.0	12.3	
11	Four-	O1–C3	77.1	19.1	
12		O3–C1	57.7	13.0	

Table 1 (*Contd.*)

Entry	Ring-closure	Ways	G_a	G_r	Structure of products
13		O2–C4	79.9	17.4	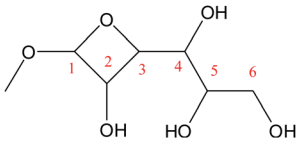
14		O4–C2	82.2	15.8	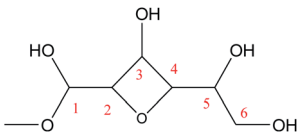
15		O3–C5	92.3	17.5	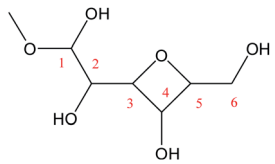
16		O5–C3	88.2	18.3	
17		O4–C6	81.3	14.8	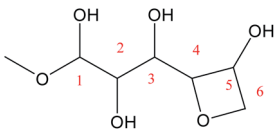
18		O6–C4	82.7	8.2	
19		O1–C4	65.6	−1.3	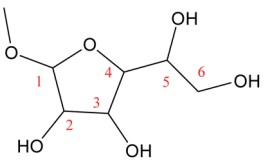
20		O4–C1	65.1	−3.5	
21		O2–C5	70.9	−4.6	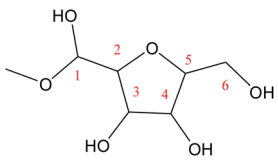
22	Five-	O5–C2	74.7	−5.5	
23		O3–C6	76.3	−0.8	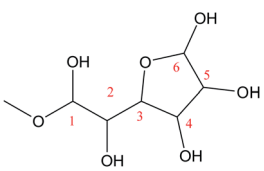
24		O6–C3	73.4	1.8	
25		O1–C5	70.3	−5.4	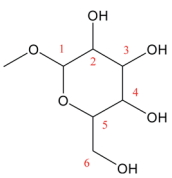
26		O5–C1	52.8	−6.5	
27	Six-	O2–C6	70.8	−7.8	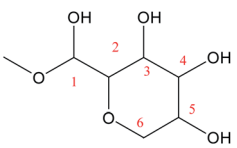
28		O6–C2	71.1	−12.0	

Å bond length. The C1 site was activated by Al^{3+} as the C1···O1H bond elongated by 0.538 Å (original 1.422 Å). In the TS4 structure, the H5 of O5 transfers to the methoxy coordinated with Al^{3+}, and the O1–H1 broke away with the coordination of Al^{3+}. The length of C1–O5 gradually decreased and MDGP was finally formed with 30.3 kcal mol^{-1}. This process is exothermic by

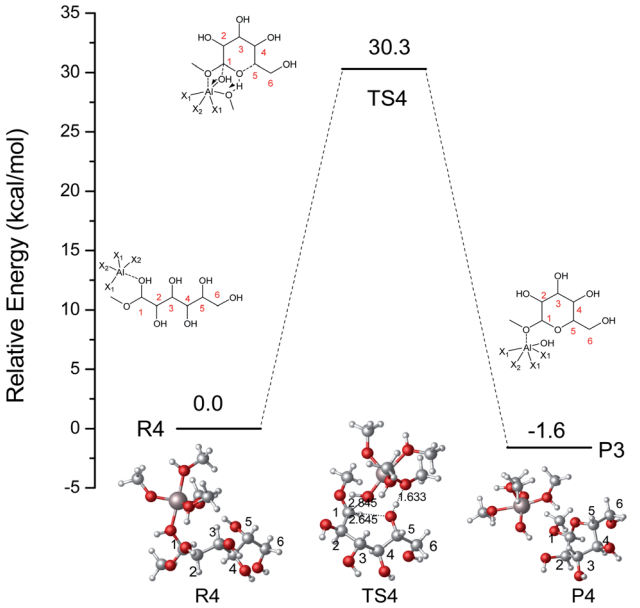

Fig. 7 The potential energy (kcal mol^{-1}) profile with the structures of reactants, transition states, and products for the O5–C1 ring-closure reaction to MDGP catalyzed by $[Al(CH_3O)_2(CH_3OH)_2]^+$. ($X_1$ = CH_3OH, X_2 = CH_3O, bond distances in Å).

1.6 kcal mol^{-1}. Comparing the energy barrier of each step, the ring-closure reaction is the overall limited step in the Fischer–Helferich glycosidation.

As a practical tool for visualizing interaction types, reduced density gradient (RDG) analysis was proposed by Yang *et al.* based on the reduced density gradient *versus* the electron density multiplied by the sign of second Hessian eigenvalue.[50] This method has been prevalently used to study non-covalent interaction in many DFT types of research.[51,52] To assess the ability of different ring-closure reactions, RDG analysis was performed for the products of five-(O4–C1) and six-(O5–C1) membered ring closure reactions as listed in Fig. 8. In the ring formation, the effects of steric hindrance will become apparent.[53,54] The red region (Fig. 8) which was plotted with a red rectangle can be classified as the steric hindrance effect in the ring closure process. The sign(λ_2)ρ of the five- and six-membered ring closure products is 0.0425 and 0.0209 a.u., respectively. It indicates that the steric effect in the middle of the five-membered ring is stronger than that of six-.

3.4 The whole glycosidation of glucose to methyl glycosides

Combining the above DFT calculations, the complete mechanism of glycosidation of glucose to methyl glycosides catalyzed by $[Al(CH_3O)_2(CH_3OH)_2]^+$ is depicted in Fig. 9 and the detailed reaction mechanism is presented in Scheme 3 based on the lowest reaction pathways by DFT calculations. The optimized XYZ coordinates of all TSs without catalyst and catalyzed by $[Al(CH_3O)_2(CH_3OH)_2]^+$ are listed in Table S2 and S3,† respectively. The first stage of the ring-opening reaction corresponds to the approach of glucose toward the active site resulting in

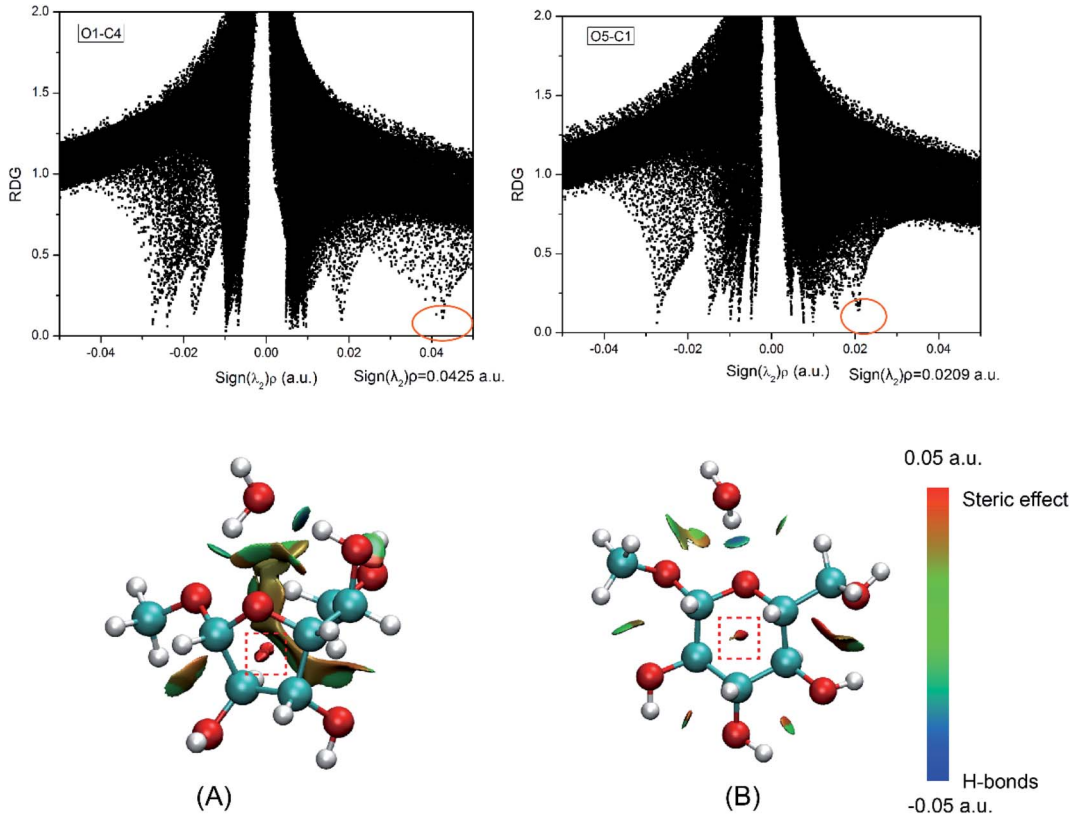

Fig. 8 RDG analysis for the (A) five-number ring and (B) six-number ring. The isosurfaces are colored on a blue–green–red scale according to values of sign (λ_2)ρ, ranging from −0.05 to 0.05 a.u. Blue indicates strong attractive interaction and red indicates steric effect.

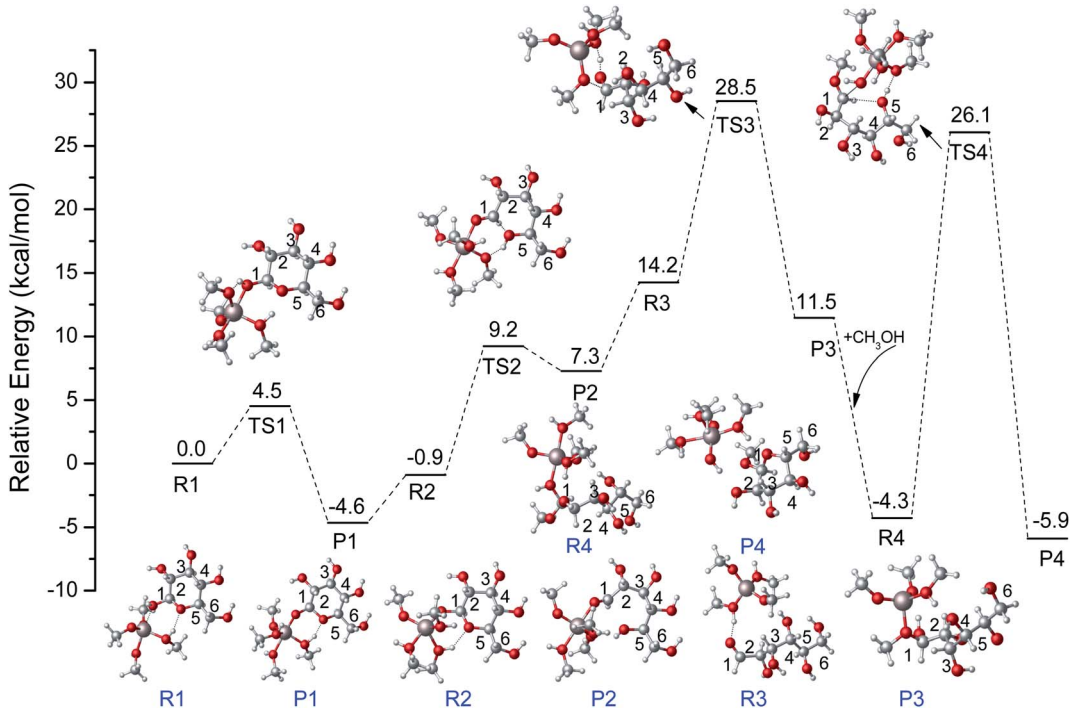

Fig. 9 The potential energy (kcal mol^{-1}) profiles for glycosidation of glucose to methyl glycosides catalyzed by $[Al(CH_3O)_2(CH_3OH)_2]^+$ at M06-2X-D3/6-311+G** level.

complex R1, in which the O1 strongly bonded to the Al^{3+} center (Al–O1 = 2.031 Å) and the O5 bonded to the methanol coordinated with Al^{3+} (OH···O5 = 1.769 Å). About 4.5 kcal mol^{-1} energy barrier needs to be overcome *via* the transition state structure of TS1. The formation of intermediate P1 where Al^{3+} coordinated with O1 of glucose will be beneficial for the following ring-opening step. Subsequently, the hydrogen of hydroxyl of methanol coordinated with Al^{3+} migrates to O5, and the reaction needs to overcome the 10.1 kcal mol^{-1} energy barrier with the C1–O5 bond cleavage. The formation of the ring-opening structure is endothermic with an energy change of 8.1 kcal mol^{-1}. The structure of P2 was the ring-opening of glucose with the Al^{3+} interacting O1 site. For the R3, it has the same 2D molecular formula as P2 through the rotation of C–C bond. They are spatial isomers without transient states. For the ring-opening step of glucose, it had been referred by the isomerism of glucose to fructose reported before.[55,56] Then, the methoxy (CH_3O) coordinated with Al^{3+} forms CH_3O–C1 bond, and the hydrogen of hydroxyl of methanol migrates to the O1 *via* TS3. The barrier of the addition reaction is 14.3 kcal mol^{-1} which is relatively higher than the ring-opening step. This step is exothermic with 2.7 kcal mol^{-1}. In the last step, the center Al^{3+} strongly coordinated with O1, the C1–O1 bond has been activated where the bond length of C1–O1 becomes longer (original 1.409 to 1.453 Å). For the TS4, the O1H will break away from C1, and the H5 transfers to the methoxy coordinated with Al^{3+}, at the same time O5–C1 bond was formed and finally generate MDGP. The energy barrier is 30.5 kcal mol^{-1} and this step is exothermic with 1.6 kcal mol^{-1}. It can be concluded that the rate-determining step is the ring closure reaction.

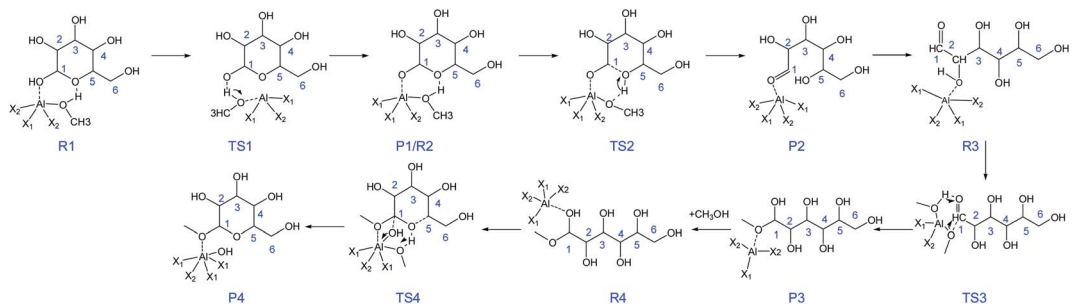

Scheme 3 The proposed mechanism for glucose to methyl glycosides in methanol solvent catalyzed by $[Al(CH_3O)_2(CH_3OH)_2]^+$. ($X_1 = CH_3OH$, $X_2 = CH_3O$).

Compared with the energy profile of no catalyst, the Al^{3+} can show a great catalytic effect in the glycosidation of glucose to MDGP, and Al^{3+} plays a critical role in the hydrogen transfer.

4. Conclusion

For the methanolysis of carbohydrates into methyl levulinate, Al-based catalysts, such as $Al_2(SO_4)_3$ and $AlPW_{12}O_{40}$ have shown great advantages in the conversion process. As a prevalent reaction, Fischer–Helferich glycosidation is easy to proceed from glucose to alkyl glucosides in an alcoholic solvent. DFT calculations have been carried out to reveal the detailed mechanism for the glycosidation of glucose to methyl glycosides by Al-based catalysts. There are mainly three steps for the Fischer–Helferich glycosidation, which are ring-opening, addition, and ring-closure steps. The Al^{3+} coordinated with methanol/methoxyl could reduce the energy barrier to some extent in the ring-opening step by transferring the proton. In the addition reaction, the electronegativity of C1 increased when the methanol was added to the C1 site. It would be beneficial for the following ring-closure step. For the ring-closure step, there are probably 28 different kinds of ways, and the O5–C1 which rendering the MDGP is more preferred with the lowest energy barrier. In the whole process of Fischer–Helferich glycosidation catalyzed by $[Al(CH_3O)_2(CH_3OH)_2]^+$, the ring-closure is the rate-determining step and the Al^{3+} coordinated with methanol/methoxyl mainly reflects on a proton shuttle to promote the reaction. A novel reaction mechanism of Fischer–Helferich glycosidation was proposed based on our DFT calculations. This work would provide basic aid to understand the mechanism of Fischer–Helferich glycosidation catalyzed by Al-based catalysts and the conversion of glucose in the alcoholic solvent.

Author contributions

Mengting Yu: methodology, writing and editing. Yao Li: funding acquisition, Cheng Zhang and Huaying Luo: project administration and resources, Chengsheng Ge: formal analysis, Xiaobin Chen and Lanlan Fu: data curation, Zhaoyang Ju and Xiaoqian Yao: review and editing. All authors discussed the results and commented on the manuscript.

Conflicts of interest

There are no conflicts of interest to declare.

Acknowledgements

This research was financially supported by the National Natural Science Foundation of China (21908222), the Key R&D Program of Zhejiang Province (2021C02031), and the Research Fund for the Quzhou University (BSYJ202015 and BSYJ202113). The work was carried out at Shanxi Supercomputing Center of Chia, and the calculations were performed on TianHe-2.

Notes and references

1 K. Alper, K. Tekin, S. Karagöz and A. J. Ragauskas, *Sustainable Energy Fuels*, 2020, **4**, 4390–4414.
2 L. T. Mika, E. Cséfalvay and Á. Németh, *Chem. Rev.*, 2018, **118**, 505–613.
3 D. Di Menno Di Bucchianico, Y. Wang, J.-C. Buvat, Y. Pan, V. Casson Moreno and S. Leveneur, *Green Chem.*, 2022, **24**, 614–646.
4 Q. Hou, X. Qi, M. Zhen, H. Qian, Y. Nie, C. Bai, S. Zhang, X. Bai and M. Ju, *Green Chem.*, 2021, **23**, 119–231.
5 Z. Ju, X. Yao, Z. Luo, M. Cao and W. Xiao, *Carbohydr. Res.*, 2020, **487**, 107882.
6 J. Liu, X. Wang, B. Yang, C. Liu, C. Xu and W. Dong, *Renewable Energy*, 2018, **120**, 231–240.
7 A. Farrán, C. Cai, M. Sandoval, Y. Xu, J. Liu, M. J. Hernáiz and R. J. Linhardt, *Chem. Rev.*, 2015, **115**, 6811–6853.
8 S. Zhu, J. Guo, X. Wang, J. Wang and W. Fan, *ChemSusChem*, 2017, **10**, 2547–2559.
9 H. Chen, J. Liu, X. Chang, D. Chen, Y. Xue, P. Liu, H. Lin and S. Han, *Fuel Process. Technol.*, 2017, **160**, 196–206.
10 F. Yu, R. Zhong, H. Chong, M. Smet, W. Dehaen and B. F. Sels, *Green Chem.*, 2017, **19**, 153–163.
11 D. Ding, J. Xi, J. Wang, X. Liu, G. Lu and Y. Wang, *Green Chem.*, 2015, **17**, 4037–4044.
12 W. Deng, L. Mi, Q. Zhang and W. Ye, *Catal. Today*, 2011, **164**, 461–466.
13 K. Chung, H. Kim, Y. Park, B. Kim, S. Kim and S. Jung, *J. Nanosci. Nanotechnol.*, 2019, **19**, 1172–1175.
14 S. Masui, Y. Manabe, K. Hirao, A. Shimoyama, T. Fukuyama, I. Ryu and K. Fukase, *Synlett*, 2019, **30**, 397–400.
15 H. Zhou, B. Wang, X. Guo, X. Zhang, X. Wei, C. Peng, D. R. MacFarlane and Y. Yuan, *Chem. Commun.*, 2018, **54**, 11969–11972.
16 W. G. Ramdani, A. Karam, K. D. O. Vigier, S. Rio, A. Ponchel and F. Jérôme, *Mol. Catal.*, 2019, **468**, 125–129.
17 L. Zhou, H. Zou, J. Nan, L. Wu, X. Yang, Y. Su, T. Lu and J. Xu, *Catal. Commun.*, 2014, **50**, 13–16.
18 K. Tominaga, K. Nemoto, Y. Kamimura, A. Yamada, Y. Yamamoto and K. Sato, *RSC Adv.*, 2016, **6**, 65119–65124.
19 Z. Ju, Y. Zhang, T. Zhao, W. Xiao and X. Yao, *ACS Sustainable Chem. Eng.*, 2019, **7**, 14962–14972.
20 M. F. He, H. Q. Fu, B. F. Su, H. Q. Yang and C. W. Hu, *J. Phys. Chem. B*, 2014, **118**, 13890–13902.
21 A. M. Norton, H. Nguyen, N. L. Xiao and D. G. Vlachos, *RSC Adv.*, 2018, **8**, 17101–17109.
22 S. Saravanamurugan, M. Paniagua, J. A. Melero and A. Riisager, *J. Am. Chem. Soc.*, 2013, **135**, 5246–5249.
23 Y. Zhang, X. Chen, X. Lyu, G. Zhao, T. Zhao, L. Han and W. Xiao, *J. Cleaner Prod.*, 2019, **215**, 712–720.
24 Y. Zhao and D. G. Truhlar, *Theor. Chem. Acc.*, 2007, **120**, 215–241.
25 S. Grimme, S. Ehrlich and L. Goerigk, *J. Comput. Chem.*, 2011, **32**, 1456–1465.
26 M. J. Frisch, G. W. Trucks, H. B. Schlegel, G. E. Scuseria, M. A. Robb, J. R. Cheeseman, G. Scalmani, V. Barone,

G. A. Petersson, H. Nakatsuji, X. Li, M. Caricato, A. V. Marenich, J. Bloino, B. G. Janesko, R. Gomperts, B. Mennucci, H. P. Hratchian, J. V. Ortiz, A. F. Izmaylov, J. L. Sonnenberg, D. Williams-Young, F. Ding, F. Lipparini, F. Egidi, J. Goings, B. Peng, A. Petrone, T. Henderson, D. Ranasinghe, V. G. Zakrzewski, J. Gao, N. Rega, G. Zheng, W. Liang, M. Hada, M. Ehara, K. Toyota, R. Fukuda, J. Hasegawa, M. Ishida, T. Nakajima, Y. Honda, O. Kitao, H. Nakai, T. Vreven, K. Throssell, J. A. Montgomery Jr, J. E. Peralta, F. Ogliaro, M. J. Bearpark, J. J. Heyd, E. N. Brothers, K. N. Kudin, V. N. Staroverov, T. A. Keith, R. Kobayashi, J. Normand, K. Raghavachari, A. P. Rendell, J. C. Burant, S. S. Iyengar, J. Tomasi, M. Cossi, J. M. Millam, M. Klene, C. Adamo, R. Cammi, J. W. Ochterski, R. L. Martin, K. Morokuma, O. Farkas, J. B. Foresman and D. J. Fox, *Gaussian*, Gaussian, Inc., Wallingford CT, 2016.

27 H. Guernon and C. Y. Legault, *Organometallics*, 2013, **32**, 1988–1994.

28 A. V. Marenich, C. J. Cramer and D. G. Truhlar, *J. Phys. Chem. B*, 2009, **113**, 6378–6396.

29 C. Gonzalez and H. B. Schlegel, *J. Chem. Phys.*, 1991, **95**, 5853–5860.

30 H. P. Hratchian and H. B. Schlegel, *Theory Appl. Comput. Chem.*, 2005, 195–249.

31 D. N. Lande, S. A. Bhadane and S. P. Gejji, *J. Phys. Chem. A*, 2017, **121**, 1814–1824.

32 T. Lu and F. Chen, *J. Comput. Chem.*, 2012, **33**, 580–592.

33 H. Liu, X. Chen, Y. Zhang, M. Lu, H. Lyu, L. Han and W. Xiao, *Energy Fuels*, 2020, **34**, 7085–7093.

34 A. J. Bridgeman, G. Cavigliasso, L. R. Ireland and J. Rothery, *J. Chem. Soc., Dalton Trans.*, 2001, 2095–2108, DOI: **10.1039/B102094N**.

35 D. D. Heard and R. Barker, *J. Org. Chem.*, 1968, **33**, 740–746.

36 R. J. Ferrier and L. R. Hatton, *Carbohydr. Res.*, 1968, **6**, 75–86.

37 A. Corma, S. Iborra, S. Miquel and J. Primo, *J. Catal.*, 1996, **161**, 713–719.

38 F. Dwight and J. Mowery, *J. Org. Chem.*, 1961, **26**, 3484–3486.

39 J. Guan, Q. Cao, X. Guo and X. Mu, *Comput. Theor. Chem.*, 2011, **963**, 453–462.

40 J. Li, J. Li, D. Zhang and C. Liu, *J. Phys. Chem. B*, 2015, **119**, 13398–13406.

41 J. Tang, X. Guo, L. Zhu and C. Hu, *ACS Catal.*, 2015, **5**, 5097–5103.

42 N. D. Tzoupanos, A. I. Zouboulis and C. A. Tsoleridis, *Colloids Surf., A*, 2009, **342**, 30–39.

43 H. Zhao, J. E. Holladay, H. Brown and Z. C. Zhang, *Science*, 2007, **316**, 1597–1600.

44 Y. Yu, C. Hu and M. M. Abu-Omar, *Bioresour. Technol.*, 2012, **116**, 190–194.

45 A. V. Demchenko, *J. Am. Chem. Soc.*, 2010, **132**, 16297.

46 Z. Ju, W. Xiao, X. Yao, X. Tan, B. A. Simmons, K. L. Sale and N. Sun, *Phys. Chem. Chem. Phys.*, 2020, **22**, 2878–2886.

47 Z. Ju, S. Feng, L. Ren, T. Lei, H. Cheng, M. Yu and C. Ge, *RSC Adv.*, 2022, **12**, 2788–2797.

48 F. Chen and T. Lu, *Acta Phys.-Chim. Sin.*, 2012, **28**, 1–18.

49 M. Miljkovic, *Carbohydrates: synthesis, mechanisms, and stereoelectronic effects*, Springer Science & Business Media, 2009.

50 E. R. Johnson, S. Keinan, P. Mori-Sánchez, J. Contreras-García, A. J. Cohen and W. Yang, *J. Am. Chem. Soc.*, 2010, **132**, 6498–6506.

51 H. Li, Y. Chang, W. Zhu, W. Jiang, M. Zhang, J. Xia, S. Yin and H. Li, *J. Phys. Chem. B*, 2015, **119**, 5995–6009.

52 H. He, S. Zhang, X. Liu, J. Wang, X. Yao and X. Zhang, *Fluid Phase Equilib.*, 2013, **360**, 169–179.

53 B. D. Marshall, A. Haghmoradi and W. G. Chapman, *J. Chem. Phys.*, 2014, **140**, 164101.

54 B. D. Marshall and W. G. Chapman, *Phys. Rev. E*, 2013, **87**, 052307.

55 J. Li, J. Li, D. Zhang and C. Liu, *J. Phys. Chem. B*, 2015, **119**, 13398–13406.

56 Y. Jing, J. Gao, C. Liu and D. Zhang, *J. Phys. Chem. B*, 2017, **121**, 2171–2178.